Proceedings of the Institute of Acoustics 'Spectral Analysis and its Use in Underwater Acoustics': Underwater Acoustics Group Conference, Imperial College, London, 29–30 April 1982

SPECTRUM ANALYSIS TECHNIQUES APPLIED TO WITHIN-PULSE SECTOR-SCANNING SONARS.

M.H.Yassaie, D.J.Creasey and N.P.Chotiros
Department of Electronic and Electrical Engineering,
University of Birmingham, P.O.Box 363, Birmingham B15 2TT, UK.

ABSTRACT This paper describes a within-pulse sector-scanning sonar receiver in which bearing information is obtained by performing a chirp-Z transform on signal samples taken from a multi-element array. The main features of the receiver are : a fast scanning speed which can be as small as 8μs,a capability of handling input signals with a dynamic range of up to 100 dB, simplicity, compactness and the use of commercially available CCD delay lines.

1.0 INTRODUCTION. When a plane wave of frequency $\omega_o/2\pi$ is incident upon an array of elements spaced a distance d in a line, the output from the k^{th} element may be written

$$x_k = A \exp (j\omega_o t + jk \cdot 2\pi d \sin\theta/\lambda) \quad (1)$$

where θ is the incident angle. The signals from each element may be phase shifted to produce cophasal waveforms so that the output from a beamformer can be written

$$V = A \cdot \sum_{k=o}^{N-1} \exp [j\omega_o t + jk (2\pi d \sin\theta/\lambda - \beta_r)] \quad (2)$$

where $\beta_r = 2\pi r/N$ = the interelement phase shift to steer the beam in a direction arcsin $\beta_r\lambda/2\pi d$. This equation may be written as

$$V = \sum_{k=o}^{N-1} x_k \exp (-2\pi jrk/N) = B_r \quad (3)$$

This will be recognised as the discrete Fourier transform (DFT) of the spatial samples x_k.(1) The process is illustrated in Fig.1a, where the instantaneous signal values for a 6-element array are plotted for sources located on the centre of the six independent beams. For the broadside target, r = 0, the six spatial samples have equal values which correspond to a zero-frequency signal. For a source centred on beam B_1 the spatially-sampled signal has one cycle across the array while sources centred on beams B_2 and B_3 give rise to two and three cycles respectively. However the spatial harmonics corresponding to beams B_5 and B_4 are identical to those obtained for B_1 and B_2 respectively. If the signals in each channel are phase shifted by $\pi/2$ radian it is possible to distinguish beams B_1 from B_5 and B_2 and B_4 because the spatial harmonics are antiphase. This is illustrated in Fig.1b.

Thus the bearing of the source may be measured by estimating the frequency of the spatial harmonic formed by the spatial samples x_k. It is essential that the in-phase and quadrature components are both available at the input to the spectrum analyser, otherwise it is impossible to distinguish between positive and negative bearings, see Fig.2.

These properties result in a common complex convolver for all the coefficients. In effect the beams are formed as a serial waveform.

Fig.5 is a block diagram of a 32-channel beamformer designed to scan a 30° sector in 32 μs with a 500 kHz carrier signal. After preamplification the signal from the k^{th} element is split into two channels each providing either a $\cos \pi k^2/32$ weighting or a $\sin \pi k^2/32$ weighting. This is done to provide the required chirp premultiplication and it is realised by an attenuator. Phase shifting networks on each channel provide a total of four channels which are then sampled to provide the real and imaginary parts of the signals into the complex convolver. This convolver is realised by four separate transversal filters. The output of the process is a waveform representing 32 samples of the spatial power spectrum.

It should be noted that the sampling process does not 'hold' the signal level. Instead the switches act merely as multiplexers and they convert parallel information into serial waveforms. If a 'hold' operation were to be used it is believed that this would reduce the dynamic range of the system.

After sampling only two channels are available. At this point dynamic range compression circuits can perform TVG or AGC functions. This has the advantage that the signal can be reduced in dynamic range to match the 40 dB or so available in the transversal filters and it is far easier to match only two compression circuits rather than a minimum of 32 for a parallel system. The input circuits, phase shifters and sampling switches can operate over dynamic ranges exceeding 100 dB.

Once the compression circuits have reduced the dynamic range to 40 dB or so the transveral filters will produce a processing gain of $10\log_{10}32$ or 15 dB. Thus the dynamic range of the output signal is around 65 dB.

In the system a 1 MHz sampling frequency is used. This produces a 32 μs scan but present CCD's would allow a 4 MHz sampling frequency or an 8 μs scan time.

Because the array elements are sampled continuously, discontinuities could cause excessive errors in the spatial power spectra. For sources centred on each beam position the spatial harmonics are continuous if the scanning frequency, f_s, and the sonar carrier frequency, f_o, are related by $mf_s = Nf_o$ where m is an integer. Thus for these targets such a scanning frequency would not cause errors in the spectral estimates. There will still be a discontinuity when the sources does not fall exactly on a beam centre. However if $mf_s = Nf_o$ the spatial signal will still be periodic and the position of the overall time window, either 'a' or 'b' in Fig.6, will not change the spectral estimate. The discontinuity itself can cause errors of up to 3.92 dB in spectral estimates.

5. SIMULATION STUDIES. Prior to building the system described the performance of the beamformer under various conditions was investigated by computer simulation studies of the system shown in Fig.6. Fig.7 shows the beam patterns obtained for targets placed at the centre of beams B_5, B_{16} and B_{29} respectively. The dotted curve indicates the usual $\sin 32X/(32\sin X)$ and is included to show the envelope expected. The output samples are plotted as solid lines ending in a dot for clarity. In Fig.8 the beam patterns are those for targets falling mid-way between two beams. Notice that there can be up to a 3.92 dB error in amplitude and that the outputs occur in adjacent beams with sidelobe levels as expected.

Normal amplitude shading will reduce sidelobe levels if required. This shading can be applied at the front end of the system together with the chirp premultiplier. As can be seen from Fig.9 the sidelobes are reduced to below -30 dB as expected.

2. SERIAL SAMPLING OF THE ARRAY ELEMENTS. So far, it has been assumed that the samples fed into the spectrum analyser would be obtained by instantaneously sampling all array elements. Fig.3 shows an array whose outputs are sampled sequentially at a rate $f_s = 1/T_s$. The only effect introduced by this serial sampling is to introduce a delay taper prior to the analyser. This will predeflect all the receiver beams by an angle

$$\theta_p = \arcsin c\, T_s/d \qquad (4)$$

where c = speed of sound in water.

By making the sampling frequency f_s equal to twice the carrier frequency f_o ($= \omega_o/2\pi$), the beam B_o will be predeflected to the edge of the scanned sector. The positions of all the beams are shown for the condition $f_s = 2f_o$ in Fig.4.

3. CHOICE OF SPECTRUM ANALYSER. For this narrow-band beamformer, the beamforming process is that of estimating the power spectrum in the waveform formed from the spatial samples. In theory any spectrum analysis method could be used but because of practical reasons it was decided to implement the process by using the chirp Z-transform(2). This hardware solution was adopted for the following reasons :

a) The transform can be realised simply in a compact form using commercially available CCD tapped-delay lines.
b) These delay-lines permit fast scanning speeds (up to 125 kHz scanning rate for a 32-channel system).
c) A wide dynamic range of input signals can be handled (up to 100 dB for an active sonar) without requiring many dynamic-range compression circuits (TVG, AGC etc) prior to the spectrum analyser. This is achieved by taking advantage of the serial nature of the chirp Z-transform.
d) The relatively poor dynamic range of the CCD elements can be overcome by using only two signal compression circuits.
e) The power consumption of CCD elements is low compared to a completely digital realisation(3).

4. IMPLEMENTATION USING THE CHIRP Z-TRANSFORM. In eqn.3 the term $-2rk$ can be replaced by $(r-k)^2 - r^2 - k^2$ and rewritten as:

$$B_r = e^{-\pi j r^2/N} \sum_{k=0}^{N-1} \left(x_k \cdot e^{-j\pi k^2/N}\right) \cdot \left(e^{-\pi j (r-k)^2/N}\right) \qquad (5)$$

The exponential term outside the summation process has unity magnitude and since only the power spectrum is of interest the term $\exp(-\pi j r^2/N)$ may be neglected. Thus to implement the transform three operations are required :

i) premultiplication of the samples x_k by a complex linear frequency-modulated signal $\exp(-j\pi k^2/n)$,
ii) the convolution, or correlation, of this new set of spatial samples with a second chirp, $\exp(-j\pi(r-k)^2/N)$, and
iii) combination of the real and imaginary parts of the convolution to form the power spectrum.

Initial inspection of eqn.5 would indicate that the process requires a separate convolver for each coefficient r. However a sampled chirp signal, $f(m)$, has the following properties for $f(m) = \exp(-m^2\pi j/N)$
$f(m) = f(m+N)$ and
$f(-m) = f(m)$.

In this type of narrow-band system large Doppler shifts might be expected to cause problems. Additionally any unknown Doppler shift would be likely to invalidate the requirement $mf_s = Nf_o$. Fig.10 shows the resulting effects on the broadside beam B_{16} for sonar-signal frequencies of 501 kHz, 505 kHz and 510 kHz with f_s equal to 1 MHz. As f_o deviates from 500 kHz an error in target position occurs. Figs.11 and 12 show the effect of changing f_o on beams B_5 and B_{29}. These results show that the errors in sidelobe levels are only significant for a 10 kHz deviation in frequency. Also for a change of up to 5 kHz the errors in beam positions are negligible. It can be concluded that the system is able to cope with fractional Doppler shifts in frequency of up to 1%.

6. COMMENTS. The beamforming system described here is presently under construction and it will be used as an instrument for further research. It is hoped also to extend the system to scan in two angular dimensions as the process appears to lend itself simply to two-dimensional scanning. Equally because of the possibility of high scanning speeds the system could be applied to other remote sensing applications other than underwater acoustics. Some forms of non-destructive testing, medical ultrasonics and radar could possibly use the technique.

7. REFERENCES

1. G.D.Bergland, "A guided tour of the Fast Fourier Transform", IEEE Spectrum, July 1979, pp 41-52.
2. L.R.Rabiner, R.W.Schafer and C.M.Rader, "The chirp Z-transform algorithm", IEEE Trans.on Audio and Electroacoustics, AD-17, 1969, pp 86-92.
3. J.F.Dix , N.Dean, J.Widdowson and J.Mavor, "Applications of c.c.ds to sonar systems" IEE Proc., Vol.127, Pt.F, No.2, April 1960, pp 125-131.

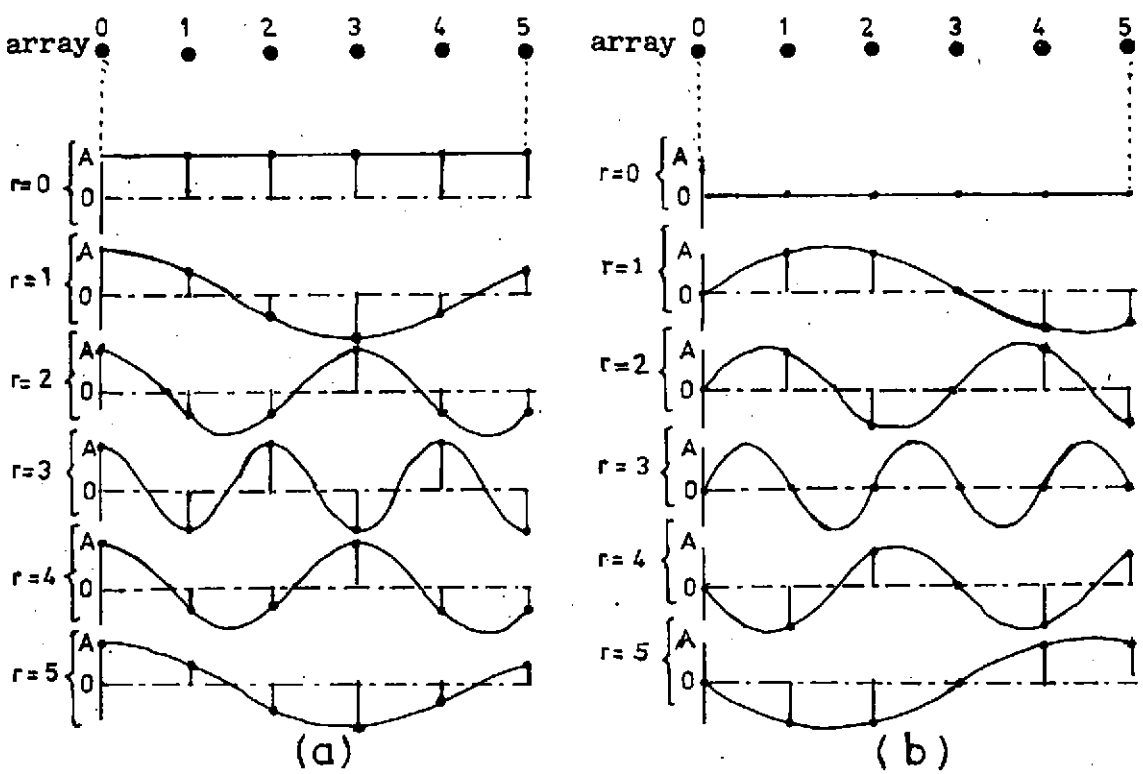

Fig.1-Instantaneous spatial samples taken from a 6-element array (a)-real parts of x_k (b)-imaginary parts of x_k .

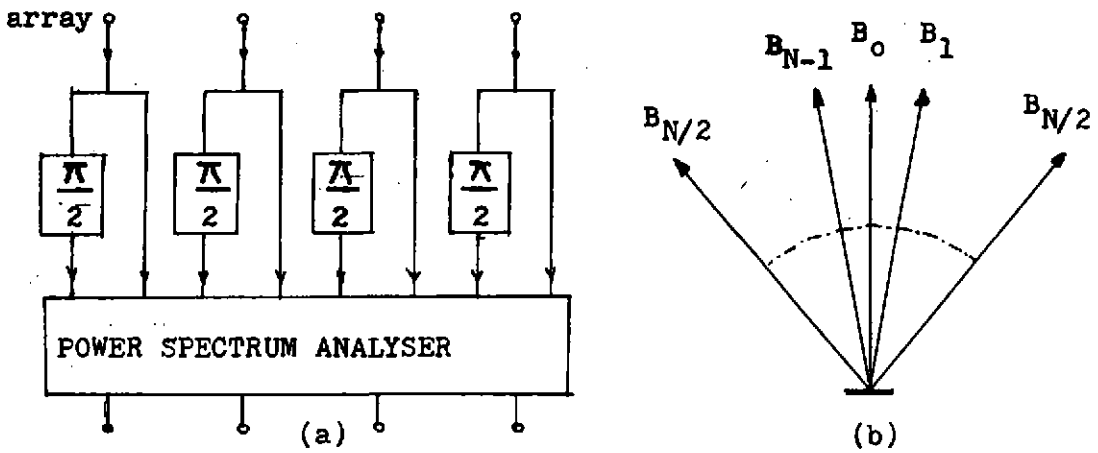

Fig.2-(a)-Beamforming using power spectrum analyser.
(b)-Beam positions.

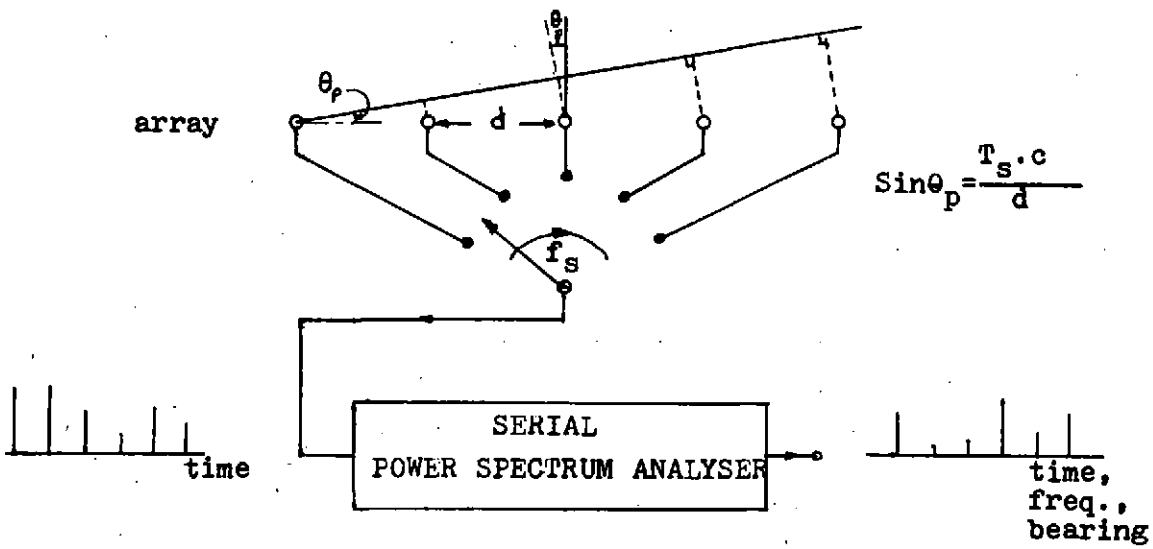

Fig.3-Effect of serial sampling of the array elements.

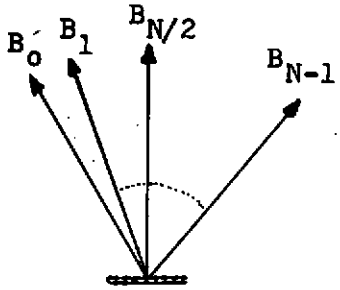

Fig.4-Beam positions for the condition $f_s=2f_o$.

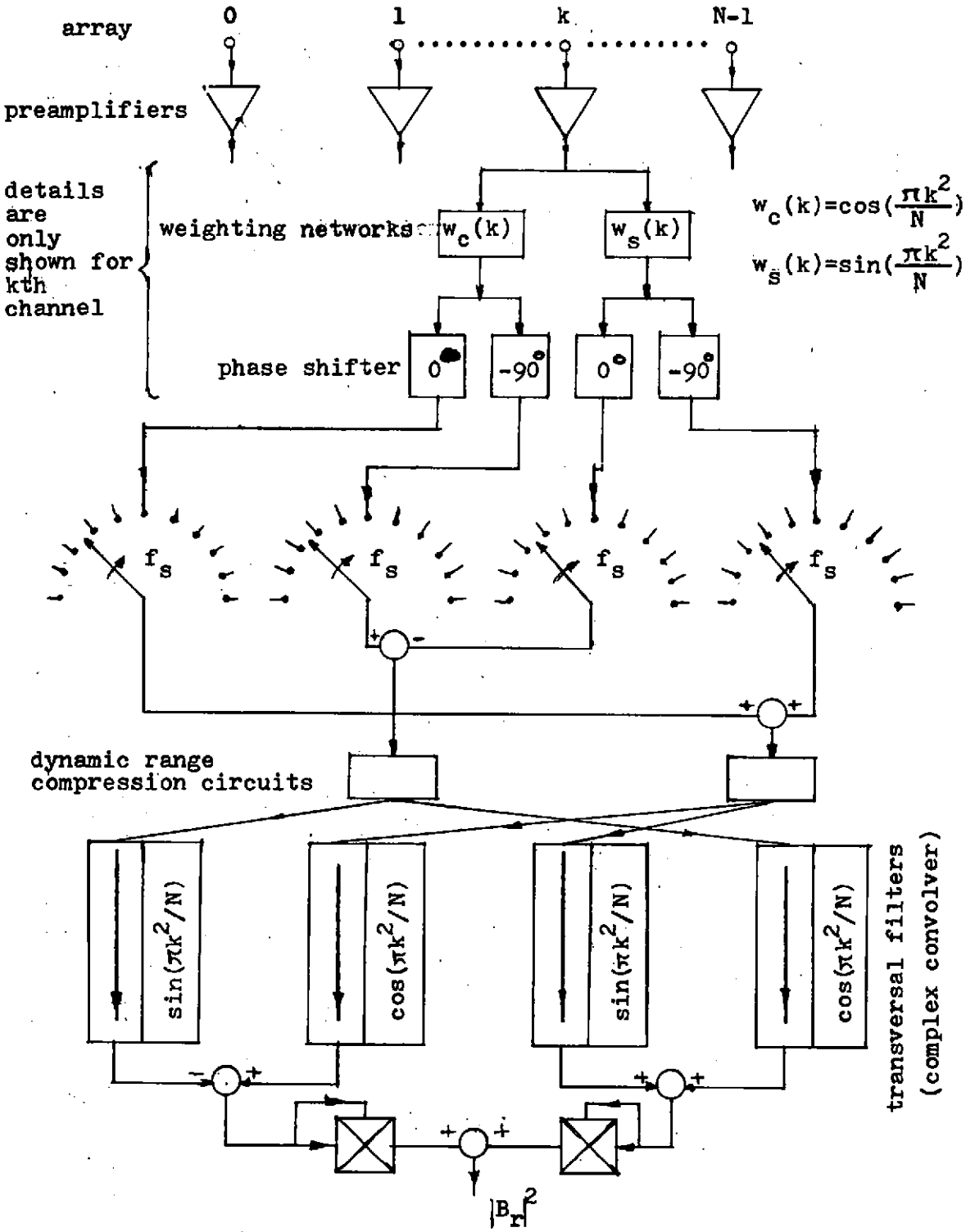

Fig.5-Block diagram of the system.

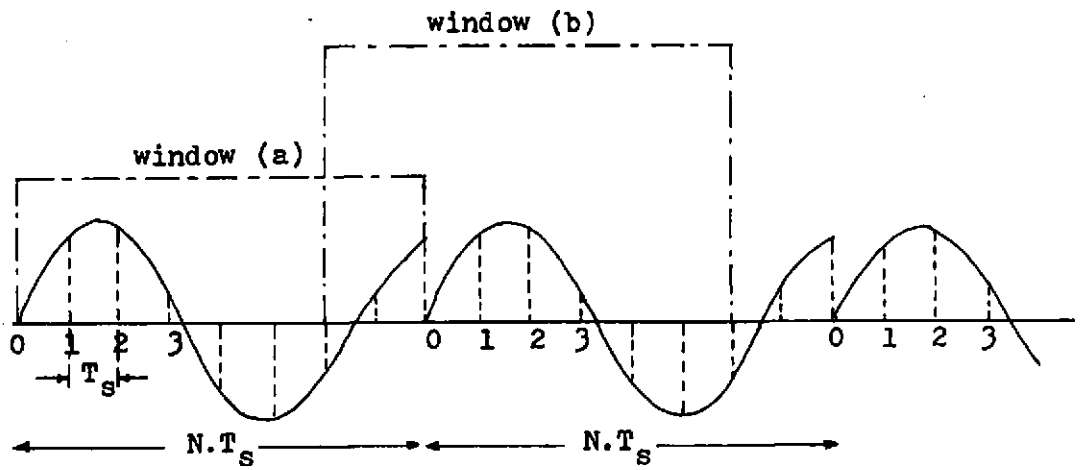

periodic if $NT_s = m.T_o$

Fig.6-Spatial waveform for a target midway between two adjacent beams.

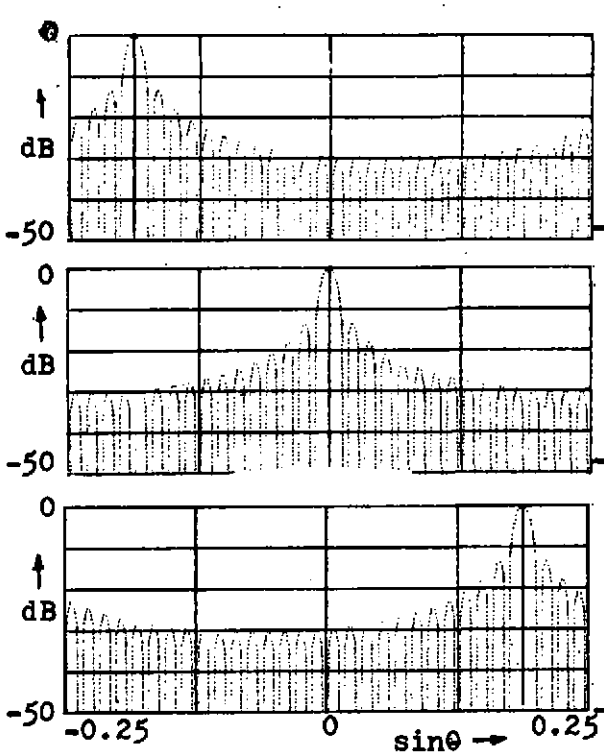

Fig.7-Beam patterns for target placed at the centre of beams B_5, B_{16}, B_{29} respectively.

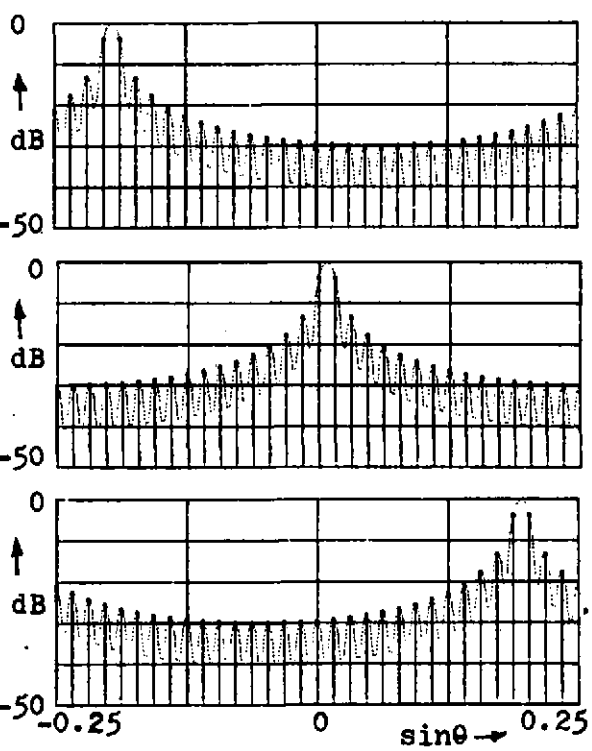

Fig.8-Beam patterns for targets midway between two beams.

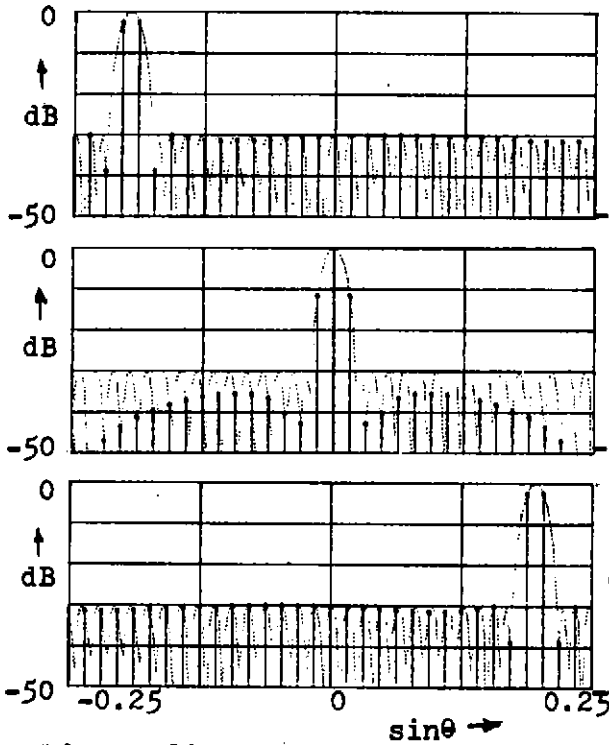

Fig.9-Effect of Dolphchebychev amplitude shading.(-30dB sidelobe)

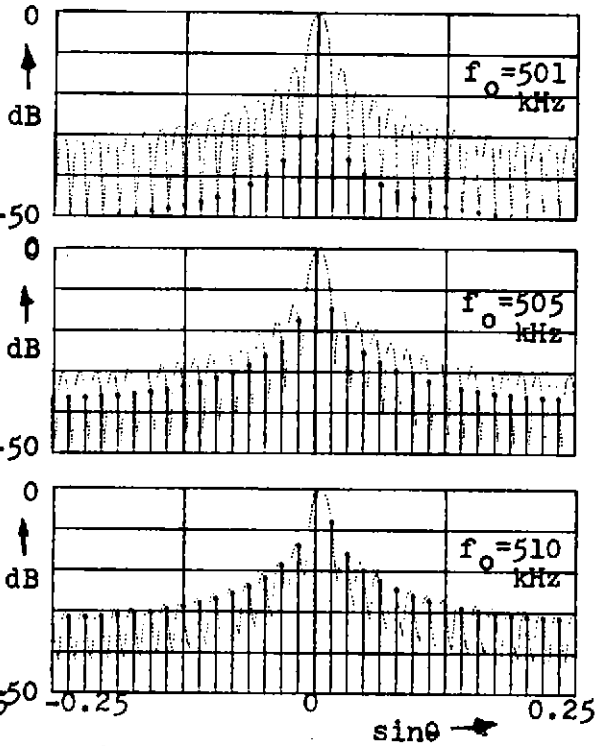

Fig.10-Effect of frequency change on the beampatterns

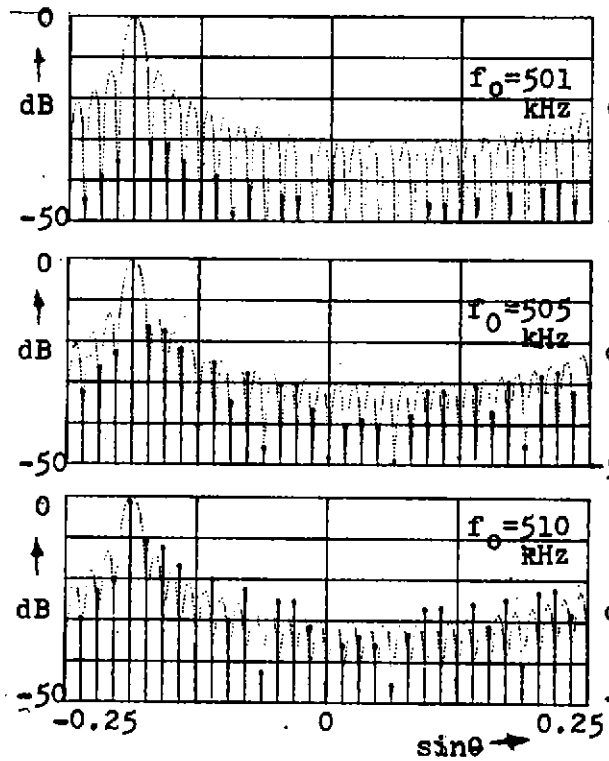

Fig.11-Effect of freq. change for targets centred at B5.

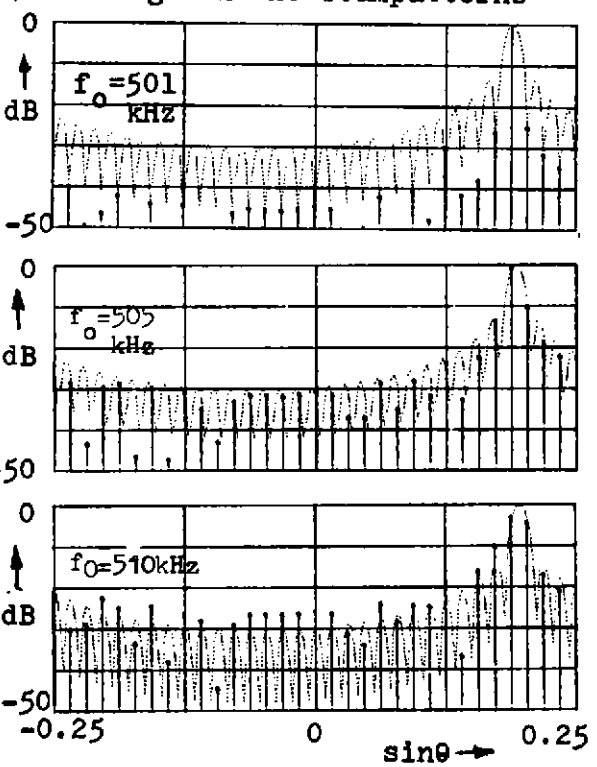

Fig.12-Effect of freq.change for targets centred at beam B29.